



RESEARCH LETTER

10.1002/2015GL064040

Key Points:

- Snow aspect ratio distributions are broad and a function of riming
- Snow orientations can have high vertical tilts that scale with air turbulence
- Precipitation retrieval algorithms may need to account for these effects

Correspondence to:

T. J. Garrett,
tim.garrett@utah.edu

Citation:

Garrett, T. J., S. E. Yuter, C. Fallgatter, K. Shkurko, S. R. Rhodes, and J. L. Endries (2015), Orientations and aspect ratios of falling snow, *Geophys. Res. Lett.*, 42, doi:10.1002/2015GL064040.

Received 30 MAR 2015

Accepted 11 MAY 2015

Accepted article online 14 MAY 2015

Orientations and aspect ratios of falling snow

Timothy J. Garrett¹, Sandra E. Yuter², Cale Fallgatter³, Konstantin Shkurko⁴, Spencer R. Rhodes², and Jason L. Endries²

¹Department of Atmospheric Sciences, University of Utah, Salt Lake City, Utah, USA, ²Marine, Earth, and Atmospheric Sciences, North Carolina State University at Raleigh, Raleigh, North Carolina, USA, ³Fallgatter Technologies, Sandy, Utah, USA, ⁴School of Computing, University of Utah, Salt Lake City, Utah, USA

Abstract Photographs of nearly 73,000 snowflakes in free fall are used to determine the aspect ratio and orientation of aggregates, moderately rimed particles, and graupel. Observations indicate that there can be a much broader range of orientation angles, with a larger median value, than has been indicated by previous observational and theoretical studies. The data show that aspect ratio depends on riming extent but that orientation is only weakly dependent on the degree of riming and on particle size. Instead, more vertical orientations for frozen particles become increasingly common with higher turbulence. The results suggest that distributions of size, fall speed, orientation, and aspect ratio may each need to be considered in order to optimize the accuracy of precipitation retrievals using microwave sensors.

1. Introduction

Microwave sensors are used to infer snowfall rates based on assumed relationships between the mass of a frozen hydrometeor and its scattering properties. Thus far, the problem has not been well constrained, in part because snow comes in a very wide variety of shapes and orientations [Liu, 2008]. The simplest approach has been to treat each individual particle as a homogenous spheroid of assumed density and orientation. Explicitly idealized snowflake shapes lead to more accurate scattering cross sections [e.g., Mishchenko, 2000; Draine and Flatau, 2008], particularly for large particle sizes or high microwave frequencies where more realistic snowflake shapes tend to have a smaller backscatter cross section than spheres of equivalent mass [Kim, 2006; Ishimoto, 2008; Casella et al., 2008].

Polarimetric radar data retrievals employ scattering models that in turn rely upon assumed distributions of particle size, aspect ratio, orientation, shape, and degree of symmetry [Vivekanandan et al., 1991; Matrosov et al., 2012; Xie et al., 2012; Melnikov and Straka, 2013; Matrosov, 2015]. There are few in situ observations of orientation and aspect ratio that have been published to date. Cloud Particle Imager data [Lawson et al., 2001] indicate that precipitation particles smaller than 1 mm have aspect ratios between 0.6 and 0.8 and that they exhibit a tendency toward larger aspect ratios at higher temperatures [Korolev and Isaac, 2003]. The canting angle of hydrometeors has not been measured directly, although laboratory measurements and theoretical calculations suggest a value of about 10° [List and Schemenauer, 1971; Klett, 1995].

This article presents observed distributions of the aspect ratios and orientations of graupel, aggregates, and moderately rimed particles up to 14 mm maximum dimension obtained with a Fallgatter Technologies Multi-Angle Snowflake Camera (MASC) [Garrett et al., 2012]. The MASC automatically photographs hydrometeors in free fall to obtain a large database of hydrometeors and their associated fall speeds. The paper builds on prior MASC results [Garrett and Yuter, 2014] that discussed the size and settling velocity distributions of snow.

2. Measurements

The measurements described here were obtained at an elevation of 2590 m mean sea level (msl) between 7 January and 22 April 2014 and between 18 December 2013 and 29 April 2014 at a field site located in Collins Gulch in Little Cottonwood Canyon within the Wasatch Mountain Range, Utah. A MASC was used to photograph hydrometeors. Three concentric cameras separated by 36° captured photographs of falling particles approximately 10 ± 1 cm distant. As hydrometeors passed two pairs of near-infrared emitters and detectors separated vertically by 32 mm, three 2700 lumen light-emitting diodes were simultaneously triggered at a maximum rate of 2 Hz. The fall speed of hydrometeors larger than about 0.1 mm was calculated from

consecutive triggers. The cameras were triggered by the lower set of triggers. The camera exposure time was set to limit motion blur. The shutter speed was 1/25,000th of a second for the outer two 1.2 MP cameras and 1/40,000th of a second for the center 5 MP camera.

Two colocated vertically pointing METEK 24.1 GHz Micro Rain Radars (MRRs) [Löffler-Mang *et al.*, 1999; Peters *et al.*, 2002] were positioned near the MASC. Data quality and sensitivity were improved using the methods of Maahn and Kollias [2012]. The minimum detectable echo of the MRR is approximately -5 dBZ. Vertical profiles of echos were obtained every 30 s at 150 m resolution for MRR1 and at 25 m resolution for MRR2. Concurrent measurements of snowfall, wind speed, temperature, and relative humidity were obtained throughout Collins Gulch. Here we focus on temperatures from Mount Baldy summit at 3350 m msl, T_{Baldy} , and Alta Base at 2590 m msl, T_{Base} .

Basic hydrometeor forms were discriminated according to their “complexity,” a parameter described in Garrett and Yuter [2014]. Because MASC images are photographs, particle forms can be distinguished from the relationship of the perimeter relative to the hydrometeor cross section [e.g., Schmitt and Heymsfield, 2014] and the average interpixel brightness variability. A perfect, homogenous circle has a complexity value of 1. It was found that the complexity parameter provides an objective means of assessing the degree of riming. Precise thresholds depend on subjective categorization and the camera resolution. Graupel appeared to be well categorized by values less than 1.35 and aggregates by values greater than 1.75 for the winter 2013 season [Garrett and Yuter, 2014]. For the winter 2014 season which used different lenses, the respective thresholds are 1.3 and 1.8. Aspect ratio is defined by the ratio of the minor axis length to the major axis length (or D_{max}) in each image, averaged across up to three in-focus images. Orientation is relative to 0° for the horizontal and is also an average. Particles with an aspect ratio of exactly 1 are assigned an orientation of 0° .

A selection of 72,966 hydrometeors was chosen on the basis of hydrometeor focus, location in the frame, and number of objects in the frame, optimizing image quality and correspondence to the measured fall speed. Median, 5th, and 95th percentile temperatures were -2.8°C , -11°C , and 1.6°C for T_{Base} and -8.8°C , -17.7°C , and -4.3°C for T_{Baldy} .

Distributions of hydrometeor size, fall speed, orientation, and aspect ratio, separated by hydrometeor type are shown in Figure 1. As described previously in Garrett and Yuter [2014], more heavily rimed particles tend to be smaller, presumably because they are more compact [Böhm, 1989]. Normalized size distributions of the particles generally take the form of a gamma function. Looking at the slope of the tail of the distribution λ (e.g., $N(D_{\text{max}}) = N_0 \exp(-\lambda D_{\text{max}})$), values range from 0.60 mm^{-1} for aggregates to 1.96 mm^{-1} for graupel.

The mode fall speed is about 1 m s^{-1} for all particles, with a bias toward slightly higher values for graupel. Notably, the fall speed distributions are more broad than in previous studies that infer well-constrained power law fits between fall speed and D_{max} [e.g., Locatelli and Hobbs, 1974; Brandes *et al.*, 2008].

Prior studies have described how particles can create a turbulent wake as they fall in still air [List and Schemenauer, 1971; Kubicek and Wang, 2012]. There is also environmental turbulence to consider. Laboratory and theoretical arguments suggest that the mean settling velocity might be many times different than the terminal velocity in still air [Good *et al.*, 2012]. Assuming that the $\sim 1 \text{ m s}^{-1}$ mode in the fall speed distribution is indicative of the true terminal fall speed, the observed spread in the fall speeds may be a consequence of interactions with ambient turbulence. Unlike instrumentation deployed in previous studies [e.g., Locatelli and Hobbs, 1974], the MASC was not located in a sheltered location. Garrett and Yuter [2014] described how larger particles tend to fall faster but that the presence of high turbulence spreads the fall speed distributions toward both lower and higher values.

The distributions of aspect ratio narrow and become more skewed toward unity as the degree of riming increases. The median aspect ratio for aggregates is 0.60, versus 0.70 for moderately rimed particles and 0.85 for graupel where the respective median values of D_{max} are 3.3 mm, 1.8 mm, and 1.2 mm. Similar aspect ratio values were obtained previously by Korolev and Isaac [2003], although for particles not larger than 1 mm.

It might be expected that particles with lower aspect ratios would experience more air resistance to rotation and have a preference for lying closer to the horizontal. Canting angles are expected to drop off exponentially as $\sin^2 \theta$ [Fraser, 1979]. The results here suggest a more complicated picture. Aggregates, which tend to have higher aspect ratios, have a slightly wider range of possible orientations. The median orientation is 35° for graupel, 35° for rimed particles, and 39° for aggregates. However, the respective modes in the distributions are 20° , 16° , and 13° , suggesting that aggregates nonetheless have a preference for the horizontal. Orientation

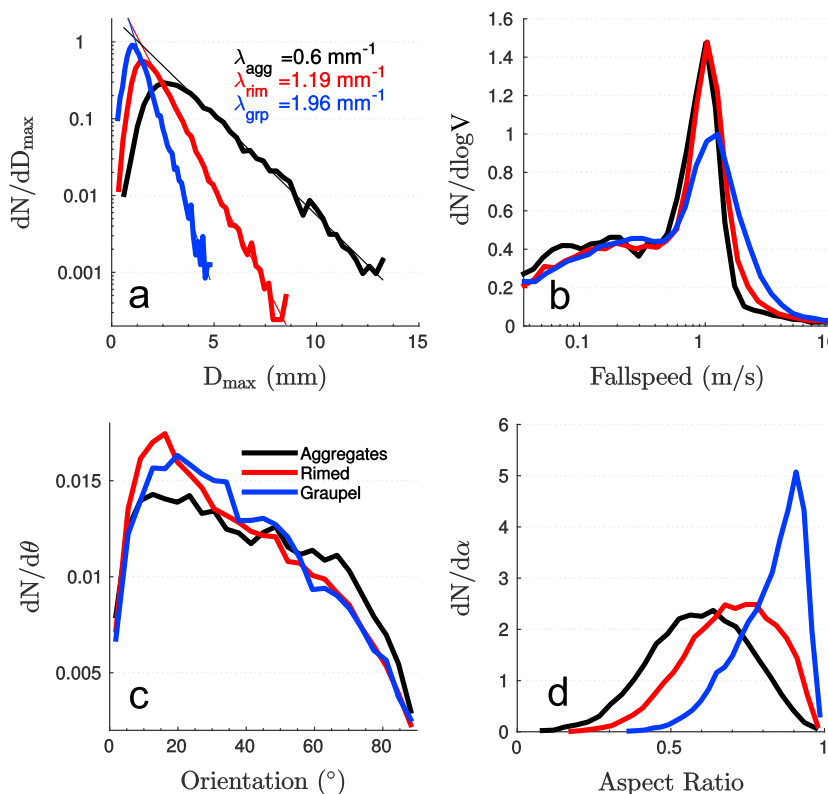


Figure 1. Normalized distributions of (a) particle maximum dimension D_{max} , (b) fall speed V , (c) orientation of the maximum dimension with respect to the horizontal θ , and (d) particle aspect ratio α defined as the ratio of the length of the minimum axis to the maximum axis. Particle types shown are aggregates (black), rimed particles (red), and graupel (blue). The value λ represents the slope of the exponential tail of the size distribution. All values represent an average over three multiangle camera views.

values of approximately 10° are what might be anticipated from prior studies [List and Schemenauer, 1971; Klett, 1995]. Here there is a weak dependence of orientation on degree of riming and a broad range of possible orientation angles.

As with the observations for fall speed described in Garrett and Yuter [2014], the reason for the broad spread of orientation values appears to be related to environmental turbulence. No direct measurement of turbulence

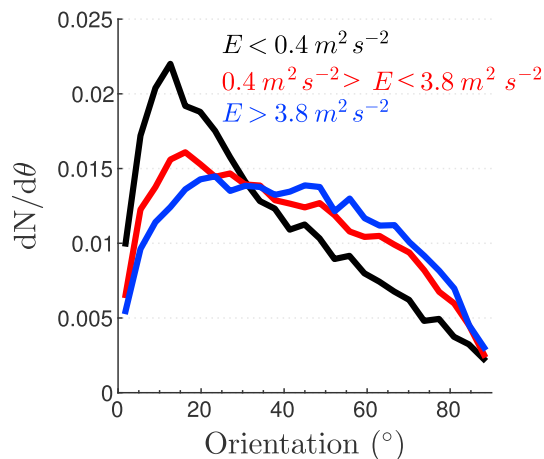


Figure 2. Orientation of frozen hydrometeors for low turbulence (black), medium turbulence (red), and high turbulence (blue).

was obtained during the field experiment; we were, however, able to infer an approximate measure from wind measurements obtained near the MASC at Alta Base. The maximum wind speed was determined from every 3 s of measurements; the average wind speed was recorded at 5 min intervals at Alta Base; gusts represent the highest 3 s values within each 5 min interval. From Schreur and Geertsema [2008], turbulence values are roughly proportional to $E = (\text{Gusts} - \text{Average Wind})^2/2$. Turbulence levels were characterized as low or high based on the upper and lower quartiles in measured distributions of E . Medium turbulence represented the middle two quartiles.

Figure 2 indicates that turbulence broadens the orientation distributions. For low turbulence conditions with $E < 0.4 \text{ m}^2 \text{ s}^{-2}$, the mode and

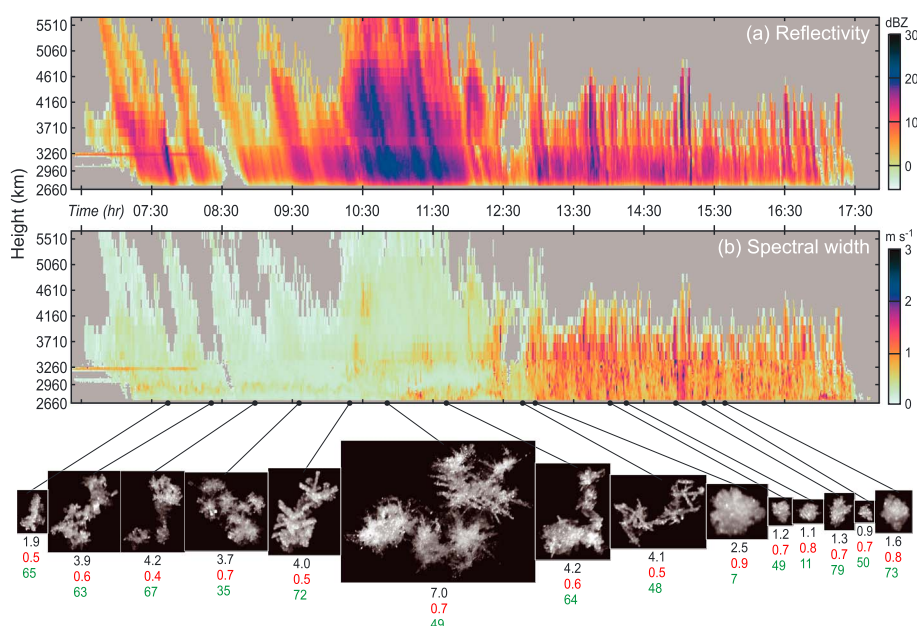


Figure 3. Time-height plots of MRR (a) radar reflectivity and (b) Doppler spectral width. Selected MASC images of larger particles are shown below the time-height plots. Numerical values under the MASC snowflake images correspond to maximum dimension (mm) in black, aspect ratio in red, and orientation (degrees) in green. The discontinuity at 3385 m altitude is where the plots transition from 25 m gate spacing to 150 m gate spacing. The two horizontal lines between 2.9 and 3.3 km altitude before 0830 UTC are radar artifacts. From 0730 to 1230 UTC, a shallow (<1 km) undulating layer of higher spectral width near 2.8 km altitude is associated with vortices forming from the interaction of ambient flow with a nearby ridge (J. Steenburgh, personal communication, 2014).

median values of the orientation are 13° and 28° . For higher turbulence with values of $E > 3.8 \text{ m}^2 \text{ s}^{-2}$, the particle orientation spread increases, and the mode and median values are 23° and 40° .

Our observations indicate that orientation does not have a strong relation to particle size. Even in low turbulence the correlation coefficient r relating particle size to orientation is < 0.03 , regardless of degree of riming.

A snow storm observed on 10 February 2014 illustrates variations in storm structure, turbulence, and surface hydrometeors that span characteristics typical of many storms at Alta, UT (Figure 3). The vertically pointing radar data reveal fall streaks of enhanced reflectivity associated with generating cells above 4 km altitude msl for the entire storm duration. During the first portion of the storm from 0730 to 1200 UTC, a mixture of mostly aggregates and rimed particles fell at the surface and values of the average Doppler spectral width (a proxy for turbulence) in the column were low. After 1300 UTC, the storm became more turbulent through nearly the entire depth of the detectable echo and mostly graupel was observed at the surface.

The 25th, 50th, and 75th percentiles for orientation were 13° , 26° , and 46° during the low column turbulence period from 0730 to 1200 UTC and 24° , 43° , and 60° during high column turbulence period from 1300 to 1700 UTC, respectively. Restricting the comparison only to aggregates, the respective percentiles were 17° , 36° , and 55° and 40° , 58° , and 67° . Higher column turbulence was associated with generally higher, more vertical particle tilts.

3. Summary

The results presented here indicate that distributions of frozen hydrometeor size and aspect ratio are clearly distinct among aggregates, moderately rimed, and graupel categories. In contrast, fall speed and orientation quantities appear to be determined more by short-term interactions with ambient air. When turbulence is high, orientation distributions are broad. Radar retrievals of snow can be sensitive to both aspect ratio and orientation [Aydin and Tang, 1997; Hogan and Westbrook, 2014]. Assuming fixed values for either of these quantities [e.g., Wood et al., 2015] may introduce added uncertainties to the determination of snow rates, much as assuming a fixed particle size when a size distribution is present.

Cloud radar depolarization ratio measurements from mountain winter storms point to aspect ratios of 0.5 ± 0.02 [Matrosov, 2015]. Combined lidar and dual polarization radar observations and Ka-band cloud radar depolarization ratio observations in winter layer clouds containing pristine planar ice indicate that crystals can fall with orientations that are very nearly horizontal [Matrosov et al., 2005; Westbrook et al., 2010]. From a more theoretical perspective, Klett [1995] has argued that even for high kinetic eddy dissipation rates of $0.1 \text{ m}^2 \text{ s}^{-3}$ (similar to what might be observed in a convective cloud), based on an inertial subrange model for turbulence, the calculated average tilt of branched plates larger than about 0.1 mm should be expected to be no more than about 10° .

Here the measured aspect ratios were higher, with median values ranging from 0.6 to 0.85 dependent on the extent of riming. The hydrometeor orientations that were observed were much higher, with a median value of 40° under high turbulence and 23° for low turbulence.

We do not have an easy theoretical explanation for the discrepancy between our results and prior studies. It is not yet well understood how nonspherical particles interact with environmental turbulence [Mandø and Rosendahl, 2010]. Klett's theoretical simplification that turbulence is steady state and isotropic may not have been appropriate at the spatial scales of snowflakes, a point the author himself acknowledged. One clue from casual visual observations of snow falling at Alta is that even under very light winds, snowflakes either flutter as they fall or their upwind side is tilted.

A possible weakness of our measurements is that the MASC, like any in situ instrument, perturbs the quantities it measures, in this case by generating its own local turbulence in the presence of horizontal winds. One test is to consider measurements of raindrops since these are generally thought to have low canting angles, even under moderate winds [Bringi et al., 2008]. The MASC is not specifically designed to measure raindrops since the instrument uses forward illumination and raindrops are highly transparent. Nonetheless, the few measurements of rain at Alta and a larger number obtained in the Salt Lake City with a white background also point to low raindrop canting angles within the MASC.

Also, preliminary computational fluid dynamics calculations indicate that when there is an incident 5 m s^{-1} horizontal flow, the MASC body generates turbulent eddies within the sample volume with peak velocities of about 0.3 m s^{-1} . Median horizontal wind speeds associated with all snowflake measurements described here were 1.9 m s^{-1} . In the 95th percentile they were 5.1 m s^{-1} . Even for the high turbulence quartile shown in Figure 2, the median and 95th percentile speeds were 3.7 m s^{-1} and 6.8 m s^{-1} .

Assuming that turbulent eddies in the sample volume scale with the wind speed near the instrument and given that unlike snowflakes, measured raindrops have low orientation angles, the contribution of instrument-generated turbulence to the orientation measurements of frozen hydrometeors may have been relatively minor. This issue will be examined more closely in future field work.

Acknowledgments

Special thanks to Daniel P. Horn for database development and Matthew A. Miller for technical support. Daniel Howlett, the Center for Snow Science at Alta, and the Alta Ski Area contributed to field operations. Beth Tully drafted Figure 3. This material is based upon the work supported by the National Science Foundation under grants 1127692, 1127759, and 1347491. The data sets used for this study are archived at <http://content.lib.utah.edu/cdm/ref/collection/uspacespace/id/10605>. T. J. Garrett, C. Fallgatter, and K. Shkurko are co-owners of Fallgatter Technologies, which manufactures the MASC.

The Editor thanks two anonymous reviewers for their assistance in evaluating this paper.

References

- Aydin, K., and C. Tang (1997), Millimeter wave radar scattering from model ice crystal distributions, *IEEE Geosci. Remote Sens. Lett.*, *35*, 140–146, doi:10.1109/36.551942.
- Böhm, H. P. (1989), A general equation for the terminal fall speed of solid hydrometeors, *J. Atmos. Sci.*, *46*, 2419–2427, doi:10.1175/1520-0469(1989)046<2419:AGEFTT>2.0.CO;2.
- Brandes, E. A., K. Ikeda, G. Thompson, and M. Schönhuber (2008), Aggregate terminal velocity/temperature relations, *J. Appl. Meteorol. Climatol.*, *47*, 2729–2736, doi:10.1175/2008JAMC1869.1.
- Bringi, V. N., M. Thurai, and D. A. Brunkow (2008), Measurements and inferences of raindrop canting angles, *Electron. Lett.*, *44*, 1425–1426, doi:10.1049/el:20082899.
- Casella, D., A. Mugnai, P. Sanò, and M. Formenton (2008), Microwave single-scattering properties of randomly oriented soft-ice hydrometeors, *Adv. Geosci.*, *17*, 79–85, doi:10.5194/adgeo-17-79-2008.
- Draine, B. T., and P. J. Flatau (2008), User guide for the Discrete Dipole Approximation Code DDSCAT 7.0, *arXiv*. [Available at <http://arxiv.org/abs/0809.0337v4>.]
- Fraser, A. B. (1979), What size of ice crystals causes halos?, *J. Opt. Soc. Am.*, *69*, 1112–1118.
- Garrett, T. J., and S. E. Yuter (2014), Measured effects of riming, temperature, and turbulence on hydrometeor fallspeed, *Geophys. Res. Lett.*, *41*, 6515–6522, doi:10.1002/2014GL061016.
- Garrett, T. J., C. Fallgatter, K. Shkurko, and D. Howlett (2012), Fall speed measurement and high-resolution multi-angle photography of hydrometeors in free fall, *Atmos. Meas. Tech.*, *5*(11), 2625–2633, doi:10.5194/amt-5-2625-2012.
- Good, G. H., S. Gerashchenko, and Z. Warhaft (2012), Intermittency and inertial particle entrainment at a turbulent interface: The effect of the large-scale eddies, *J. Fluid Mech.*, *694*, 371–398, doi:10.1017/jfm.2011.552.
- Hogan, R. J., and C. D. Westbrook (2014), Equation for the microwave backscatter cross section of aggregate snowflakes using the self-similar Rayleigh-Gans approximation, *J. Atmos. Sci.*, *71*(9), 3292–3301, doi:10.1175/JAS-D-13-0347.1.
- Ishimoto, H. (2008), Radar backscattering computations for fractal-shaped snowflakes, *J. Meteorol. Soc. Jpn.*, *86*, 459–469.

- Kim, M.-J. (2006), Single scattering parameters of randomly oriented snow particles at microwave frequencies, *J. Geophys. Res.*, *111*, D14201, doi:10.1029/2005JD006892.
- Klett, J. D. (1995), Orientation model for particles in turbulence, *J. Atmos. Sci.*, *52*(12), 2276–2285, doi:10.1175/1520-0469(1995)052<2276:OMFPIT>2.0.CO;2.
- Korolev, A., and G. Isaac (2003), Roundness and aspect ratio of particles in ice clouds, *J. Atmos. Sci.*, *60*(15), 1795–1808, doi:10.1175/1520-0469(2003)060<1795:RAAROP>2.0.CO;2.
- Kubicek, A., and P. K. Wang (2012), A numerical study of the flow fields around a typical conical graupel falling at various inclination angles, *Atmos. Res.*, *118*, 15–26, doi:10.1016/j.atmosres.2012.06.001.
- Lawson, R. P., B. A. Baker, C. G. Schmitt, and T. L. Jensen (2001), An overview of microphysical properties of Arctic clouds observed in May and July 1998 during FIRE ACE, *J. Geophys. Res.*, *106*, 14,989–15,014, doi:10.1029/2000JD900789.
- List, R., and R. S. Schemenauer (1971), Free-fall behavior of planar snow crystals, conical graupel and small hail, *J. Atmos. Sci.*, *28*(1), 110–115, doi:10.1175/1520-0469(1971)028<0110:FFBOPS>2.0.CO;2.
- Liu, G. (2008), A database of microwave single-scattering properties for nonspherical ice particles, *Bull. Am. Meteorol. Soc.*, *89*, 1563–1570.
- Locatelli, J. D., and P. V. Hobbs (1974), Fall speeds and masses of solid precipitation particles, *J. Geophys. Res.*, *79*, 2185–2197, doi:10.1029/JC079i015p02185.
- Löffler-Mang, M., M. Kunz, and W. Schmid (1999), On the performance of a low-cost K-band doppler radar for quantitative rain measurements, *J. Atmos. and Ocean. Tech.*, *16*, 379–387, doi:10.1175/1520-0426(1999)016<0379:OTPOAL>2.0.CO;2.
- Maahn, M., and P. Kollias (2012), Improved Micro Rain Radar snow measurements using Doppler spectra post-processing, *Atmos. Meas. Tech.*, *5*(11), 2661–2673, doi:10.5194/amt-5-2661-2012.
- Mandø, M., and L. Rosendahl (2010), On the motion of non-spherical particles at high Reynolds number, *Powder Technol.*, *202*, 1–13, doi:10.1016/j.powtec.2010.05.001.
- Matrosov, S. Y. (2015), Evaluations of the spheroidal particle model for describing cloud radar depolarization ratios of ice hydrometeors, *J. Atmos. Oceanic Technol.*, *32*, 865–879, doi:10.1175/JTECH-D-14-00115.1.
- Matrosov, S. Y., R. F. Reinking, and I. V. Djalalova (2005), Inferring fall attitudes of pristine dendritic crystals from polarimetric radar data, *J. Atmos. Sci.*, *62*(1), 241–250.
- Matrosov, S. Y., G. G. Mace, R. Marchand, M. D. Shupe, A. G. Hallar, and I. B. McCubbin (2012), Observations of ice crystal habits with a scanning polarimetric W-band radar at slant linear depolarization ratio mode, *J. Atmos. Oceanic Technol.*, *29*(8), 989–1008, doi:10.1175/JTECH-D-11-00131.1.
- Melnikov, V., and J. M. Straka (2013), Axis ratios and flutter angles of cloud ice particles: Retrievals from radar data, *J. Atmos. Oceanic Technol.*, *30*(8), 1691–1703, doi:10.1175/JTECH-D-12-00212.1.
- Mishchenko, M. I. (2000), Calculation of the amplitude matrix for a nonspherical particle in a fixed orientation, *Appl. Opt.*, *39*(6), 1026–1031, doi:10.1364/AO.39.001026.
- Peters, G., B. Fischer, and T. Andersson (2002), Rain observations with a vertically looking Micro Rain Radar (MRR), *Boreal Environ. Res.*, *7*, 353–362.
- Schmitt, C. G., and A. J. Heymsfield (2014), Observational quantification of the separation of simple and complex atmospheric ice particles, *Geophys. Res. Lett.*, *41*, 1301–1307, doi:10.1002/2013GL058781.
- Schreier, B. W., and G. Geertsema (2008), Theory for a TKE based parameterization of wind gusts, *HIRLAM Newsl.*, *54*, 177–188.
- Vivekanandan, J., W. Adams, and V. Bringi (1991), Rigorous approach to polarimetric radar modeling of hydrometeor orientation distributions, *J. Appl. Meteorol.*, *30*(8), 1053–1063, doi:10.1175/1520-0450(1991)030<1053:RATPRM>2.0.CO;2.
- Westbrook, C. D., A. J. Illingworth, E. J. O'Connor, and R. J. Hogan (2010), Doppler lidar measurements of oriented planar ice crystals falling from supercooled and glaciated layer clouds, *Q. J. R. Meteorol. Soc.*, *136*(646), 260–276, doi:10.1002/qj.528.
- Wood, N. B., T. S. L'Ecuyer, A. J. Heymsfield, and G. L. Stephens (2015), Microphysical constraints on millimeter-wavelength scattering properties of snow particles, *J. Appl. Meteorol. Climatol.*, *54*, 909–931, doi:10.1175/JAMC-D-14-0137.1.
- Xie, X., U. Löhnert, S. Kneifel, and S. I. Crewell (2012), Snow particle orientation observed by ground-based microwave radiometry, *J. Geophys. Res.*, *117*, D02206, doi:10.1029/2011JD016369.